Size-dependent recycling of membrane clusters

S. ALEX RAUTU[1,2], GEORGE ROWLANDS[1] and MATTHEW S. TURNER[1,3]

[1] *Department of Physics, University of Warwick - Coventry, CV4 7AL, UK*
[2] *Simons Centre for the Study of Living Machines, National Centre for Biological Sciences (TIFR)*
Bellary Road, Bangalore 560065, India
[3] *Centre for Complexity Science, University of Warwick - Coventry, CV4 7AL, UK*

Abstract – The role of recycling in the control of membrane domains is a contentious issue and currently an open research question. In this context, we study the coarsening of strongly microphase-separated membrane domains in the presence of recycling of material. The dynamics of cluster size distribution is studied under both scale-free and size-dependent recycling. Closed-form solutions to the steady-state distribution and its associated moments are found in both cases. For the size-independent case, the time evolution of the moments is analytically obtained, providing exact results for their corresponding relaxation times. Since these moments and relaxation times are measurable quantities that may be determined by comparison with experimental data, our results provide a framework with which to understand and assess the interplay between membrane recycling and domain formation.

Biomembranes are highly dynamic two-dimensional systems [1], consisting of many different lipids and proteins, that are continuously exchanged with the rest of the living cell by the secretion and absorption of vesicles of approximately 50–200 nm in diameter [2]. This cellular recycling of membranes leads to a complete turnover of its constituents in about 9–12 minutes [3]. In addition, the membrane components are found to be inhomogeneously distributed [4–6], where certain lipids and proteins cluster into small-scale domains with a radius of few tens of nanometers [7–10]. These supermolecular structures are free to diffuse throughout the membrane, coalescing into larger domains as they meet [7]. They are believed to be involved in controlling various biological processes, such as signal transduction, protein sorting, and endocytosis [10]. As lipid phase separation can occur in model systems of multi-component membranes, the clusters observed in living cells have often been linked to microphase-separated lipid domains [11]. Nonetheless, the characteristic size of the latter is much larger than the nanoscale clusters found *in vivo*. This is expected as phase separation in a two-component mixture manifests itself by the appearance of separated domains (below a critical temperature), which then grow until they reach the size of the system, without any intermediate stable sizes [12].

This simple thermodynamic argument makes the formation of membrane nano-domains somewhat surprising. A number of mechanisms have been put forth to explain their sub-micron scale [10]. This includes the effects due to cytoskeleton pinning, binding of cross-linkers, or extracellular adhesion [4], which limit through their attachment the growth of clusters [13]. Moreover, their growth may also be avoided if there is a repulsion between domains as they encounter each other, such as electrostatics [14] and membrane-mediated interactions induced by hydrophobic mismatch [15–17] or by curvature [18,19]. Another hypothesis proposes that the membrane nano-clusters are a two-dimensional microemulsion caused either by an explicit *edge*-actant [20–23], reducing the line tension associated with the domain, or a result of a structural modulation in the membrane properties [24], *e.g.*, the interplay between membrane composition and its curvature [25–28]. Others have hypothesized that these sub-micron heterogeneities can be viewed as near-critical fluctuations in the membrane composition [29,30].

All of the above mechanisms assume that the system is in thermodynamic equilibrium. However, membranes in living cells are active systems [31], which can be driven far from equilibrium, *e.g.*, by cytoskeleton processes [32] and membrane recycling [33]. The latter
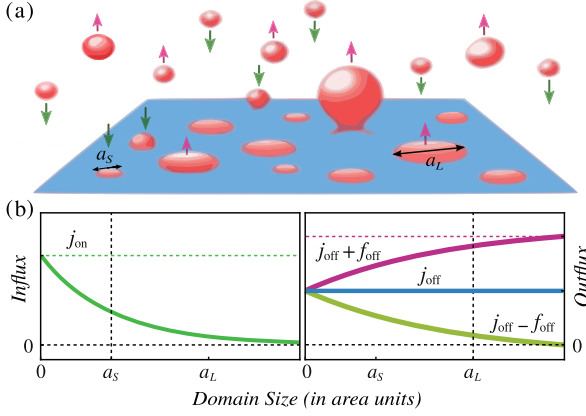
(a)

(b)

Domain Size (in area units)

Fig. 1: (Color online) (a) Schematic diagram of a planar membrane that is composed of two species, depicted by blue and red colors. The latter constituent phase-separates into membrane domains of different sizes that range between the characteristic areas $a_S \simeq 10\,\mathrm{nm}^2$ and $a_L \simeq 10^4\,\mathrm{nm}^2$. Beside their in-plane diffusive dynamics, the membrane is subjected to a continuous recycling, where the domains are brought to (green downward arrows) and removed from (pink upward arrows) the membrane through the transport of various vesicles. (b) Diagram of the membrane recycling scheme, where domains are injected into the membrane at random with a flux $j_{\mathrm{on}}\exp(-a/a_S)/a_S$. Also, they are randomly removed from the membrane with a constant rate j_{off} (blue), as well as an explicit size-dependent removal rate $f_{\mathrm{off}}[1 - \exp(-a/a_L)]$, where $f_{\mathrm{off}} > 0$ is depicted by the purple curve, plateauing to $j_{\mathrm{off}} + f_{\mathrm{off}}$, and $f_{\mathrm{off}} < 0$ is plotted in green, decreasing at large a to $j_{\mathrm{off}} - f_{\mathrm{off}}$. Since the outward rate cannot be negative, we restrict to $|f_{\mathrm{off}}| > j_{\mathrm{off}}$.

has been quantitatively studied by means of reaction-diffusion equations [34–38] and Smoluchowski coagulation equations [39–41]. Heuristically, the effect of recycling consists in a decrease of the domain lifetime, reducing the chance of a micro-sized aggregate to form as the recycling rate is increased.

In this letter, we study the role of membrane recycling in the formation and regulation of nano-clusters. We develop a continuum coagulation theory of the domain dynamics under a continuous exchange of membrane components with an external (or internal) reservoir [39–41]. In contrast to the previous studies of Smoluchowski coagulation processes [39–46], the active recycling terms (sources and sinks) are chosen to be sized-dependent. This is of biological significance, as certain recycling pathways target domains from a highly specific range of sizes [6,31,47–49].

We consider an infinite planar membrane populated by two membrane species, which undergo phase separation, giving rise to domains of various sizes as shown in fig. 1. Hereinafter, the scission events are assumed to be rare, corresponding to a regime of large line tension associated with the periphery of the domain. This line tension characterizes the energy cost for having a finite interface between the different phases. In the case of microphase separating components the regime of interest is high line

tension, while the low tension case resembles a gas of non-interacting (mostly monomeric) clusters. Thus, the kinetics of the aggregates is dominated by the fusion events [39]. Under a continuous recycling, the mean-field dynamics of the domain size distribution is governed by [44]

$$\frac{\partial \mathcal{P}}{\partial t} = \mathcal{R}(a,t) - \int_0^\infty \mathcal{G}(a,a')\mathcal{P}(a,t)\mathcal{P}(a',t)\,\mathrm{d}a'$$
$$+ \frac{1}{2}\int_0^a \mathcal{G}(a,a')\mathcal{P}(a',t)\mathcal{P}(a-a',t)\,\mathrm{d}a', \quad (1)$$

where $\mathcal{P}$ is a density function at time t for the number-per-area of domains of size a (in area units).

By assuming that two distinct membrane domains coalesce whenever they come into contact through diffusion, the kernel $\mathcal{G}(a,a')$ in eq. (1) can be regarded in the dilute limit as a constant proportional to the diffusion coefficient D of a typical membrane cluster. The latter depends only weakly (logarithmically) on the domain size a, provided that $a \lesssim a_{\mathrm{SD}}$, where a_{SD} is the area corresponding to the Saffman-Delbrück length [50]. Since this is typically found to be $a_{\mathrm{SD}} \simeq 10^5$–$10^6\,\mathrm{nm}^2$, the size-dependence of the fusion rate can be neglected throughout, as the clusters of interest are smaller than a_{SD} (see fig. 1), and those greater than a_{SD} are exponentially suppressed. Since the diffusion constant is the only parameter that describes the intramembrane dynamics, $\mathcal{G}$ is chosen to be identically $D \simeq 10^5\,\mathrm{nm}^2/\mathrm{s}$, fixing the time scale in this model. Here, $\mathcal{R}(a,t)$ is a function that controls the recycling, *i.e.*,

$$\mathcal{R}(a,t) = \frac{j_{\mathrm{on}}}{a_S}e^{-\frac{a}{a_S}} - \left[j_{\mathrm{off}} + f_{\mathrm{off}}\left(1 - e^{-\frac{a}{a_L}}\right)\right]\mathcal{P}(a,t), \quad (2)$$

where single domains are brought to the membrane at random with a flux j_{on} and a size drawn from an normalized exponential distribution. Here, a_S is the characteristic size of domains that are injected into the membrane, and it is henceforth used to set area scale in our model. Its value depends on the specific mechanism of recycling at hand. Nonetheless, in most biological cases, the recruitment of components to the membrane occurs at a monomeric level (*e.g.*, single proteins), and thus we choose $a_S \simeq 10\,\mathrm{nm}^2$. Moreover, entire domains are stochastically removed irrespective of their size with a constant rate j_{off}. In addition to this, an explicit size-dependent outward flux is included, where the removal rate f_{off} is exponentially small for domain sizes $a \lesssim a_L \simeq 10^4\,\mathrm{nm}^2$ (note that this is also smaller than a_{SD}). Depending on its sign, this could lead to an enhanced recycling at large scales if $f_{\mathrm{off}} > 0$, or a reduction if $f_{\mathrm{off}} < 0$. However, in the latter case, f_{off} cannot be larger in magnitude than j_{off}, so that the overall outward flux remains non-negative, as shown in fig. 1(b). The former scenario ($f_{\mathrm{off}} > 0$) is perhaps of greater biological relevance, due to the size associated with the endosomes, which are vapoured in the phase-separated component [6]. For example, this has been observed for the recycling of E-cadherin clusters, where dynamin-dependent endocytosis targets large domains, inducing a sharp size cut-off past a critical size [47–49].

To understand the solution of eq. (1) we first focus on the size-independent recycling scheme, namely $f_{\text{off}} = 0$. This proves to be tractable in Laplace space [51], where we define the dimensionless (integral transform) function

$$\hat{\mathcal{P}}(\lambda, t) = a_S \int_0^\infty \mathcal{P}(a, t) e^{-a\lambda/a_S}\, \mathrm{d}a. \qquad (3)$$

For clarity, it is helpful to define the following rescaled quantities at the outset: $\tau = tD/a_S$, $J_{\text{on}} = j_{\text{on}} a_S^2/D$, and $J_{\text{off}} = j_{\text{off}} a_S/D$. Therefore, this yields a nonlinear differential equation of the form

$$\frac{\partial \hat{\mathcal{P}}}{\partial \tau} = \frac{J_{\text{on}}}{1 + \lambda} - [\rho(\tau) + J_{\text{off}}]\hat{\mathcal{P}}(\lambda, \tau) + \frac{1}{2}\hat{\mathcal{P}}^2(\lambda, \tau), \qquad (4)$$

where $\rho(\tau) = \hat{\mathcal{P}}(\lambda = 0, \tau)$ is the total number-per-area of clusters (non-dimensionalised by a_S). Furthermore, by evaluating eq. (4) at $\lambda = 0$, we find that

$$\frac{\partial \rho}{\partial \tau} = J_{\text{on}} - J_{\text{off}}\rho(\tau) - \frac{1}{2}\rho^2(\tau). \qquad (5)$$

By using the initial condition $\rho_0 = \rho(\tau = 0)$, the solution to the above equation can be written, see Supplementary Material `Supplementarymaterial.pdf` (SM), as follows:

$$\rho(\tau) = \mathcal{Q}_\infty \frac{(\rho_0 + J_{\text{off}}) + \mathcal{Q}_\infty \tanh[\frac{\tau \mathcal{Q}_\infty}{2}]}{(\rho_0 + J_{\text{off}}) \tanh[\frac{\tau \mathcal{Q}_\infty}{2}] + \mathcal{Q}_\infty} - J_{\text{off}}, \qquad (6)$$

where $\mathcal{Q}_\infty = \sqrt{J_{\text{off}}^2 + 2J_{\text{on}}}$. To find $\hat{\mathcal{P}}(\lambda, \tau)$, we define a function $\psi(\lambda, \tau) = \rho(\tau) - \hat{\mathcal{P}}(\lambda, \tau)$, which by substitution into eq. (4) yields the following equation:

$$\frac{\partial \psi}{\partial \tau} = \frac{\lambda J_{\text{on}}}{1 + \lambda} - J_{\text{off}}\psi(\lambda, \tau) - \frac{1}{2}\psi^2(\lambda, \tau). \qquad (7)$$

This has the same form as before, and its solution is

$$\psi(\lambda, \tau) = \mathcal{Q}_\lambda \frac{(\psi_0(\lambda) + J_{\text{off}}) + \mathcal{Q}_\lambda \tanh[\frac{\tau \mathcal{Q}_\lambda}{2}]}{(\psi_0(\lambda) + J_{\text{off}}) \tanh[\frac{\tau \mathcal{Q}_\lambda}{2}] + \mathcal{Q}_\lambda} - J_{\text{off}}, \qquad (8)$$

where $\psi_0(\lambda) = \psi(\lambda, \tau = 0)$ and $\mathcal{Q}_\lambda = \sqrt{J_{\text{off}}^2 + \frac{2\lambda}{1+\lambda}J_{\text{on}}}$. Higher order moments of $\mathcal{P}$ can be determined by differentiating $\hat{\mathcal{P}}(\lambda, \tau)$, or equivalently $-\psi(\lambda, \tau)$, with respect to λ and then evaluating at $\lambda = 0$. Particularly, its first moment $\phi(\tau) = \int_0^\infty a\mathcal{P}(a, \tau)\mathrm{d}a = -\frac{\partial}{\partial \lambda}\hat{\mathcal{P}}(\lambda = 0, \tau)$, corresponding to the area-fraction of domains, is given by

$$\phi(\tau) = \frac{J_{\text{on}}}{J_{\text{off}}}\left[1 - e^{-\tau J_{\text{off}}}\left(1 - \frac{J_{\text{off}}}{J_{\text{on}}}\phi_0\right)\right], \qquad (9)$$

where $\phi_0 = \frac{\partial}{\partial \lambda}\psi_0(\lambda = 0)$. This allows us to find the time evolution of the mean domain size $\mathcal{A}(\tau) = a_S\phi(\tau)/\rho(\tau)$. Similarly, the second moment, i.e. $\sigma(\tau) = \frac{\partial^2}{\partial \lambda^2}\hat{\mathcal{P}}(\lambda = 0, \tau)$, can also be computed with the initial value σ_0 (see SM). Hence, this also gives us the full dynamics of the standard deviation, $\mathcal{W}(\tau) = a_S\sqrt{\sigma(\tau)/\rho(\tau) - \phi^2(\tau)/\rho^2(\tau)}$, that is associated to the density $\mathcal{P}$ of membrane clusters.
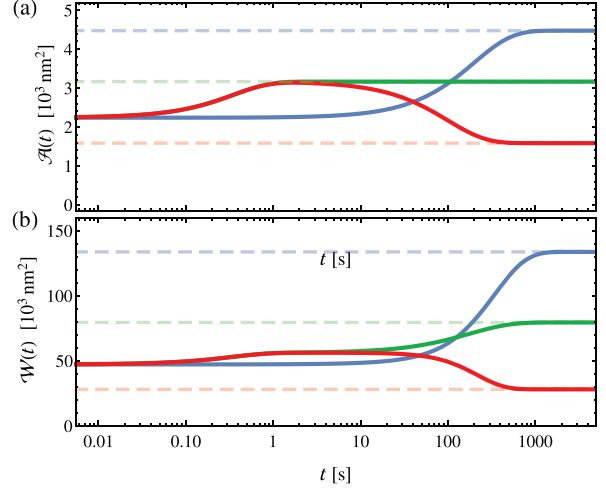

Fig. 2: (Color online) (a) Dynamics of the mean area $\mathcal{A}(t)$ of clusters, and (b) its associated standard deviation $\mathcal{W}(t)$. The initial conditions are set by considering a scenario where a step-change at $t = 0$ is made in either J_{on} or J_{off} after the system has reached its steady state. Choosing the typical physiological rates, $J_{\text{on}} = 10^{-7}$ and $J_{\text{off}} = 10^{-6}$, we make the following step-like changes: 50% decrease in J_{off} (blue); 50% decrease in J_{on} (red); and 50% decrease in both J_{on} and J_{off} (green). Due to these perturbations the system reaches a new steady state after a transient time; see the dashed lines (same colour convention).

So far, the dynamics of the moments $\rho(\tau)$, $\phi(\tau)$ and $\sigma(\tau)$ has been analytically found in terms of the initial (arbitrary) values ρ_0, ϕ_0, and σ_0, respectively. These terms can be fixed by considering that the density $\mathcal{P}$ at $\tau = 0$ is given by a steady-state configuration with the rates J_{on} and J_{off}. In fig. 2, we show how the entire system will relax after an initial (step-like) perturbation in the values of the recycling rates. Namely, we compute the response of $\mathcal{A}$ and $\mathcal{W}$ to a decrease by $\alpha = 50\%$ in J_{on} (red), or a reduction by $\beta = 50\%$ in J_{off} (blue), or by simultaneously decreasing both flux rates by 50% (green). This shows that diminishing the removal rate J_{off} leads to a monotonic increase in both $\mathcal{A}$ and $\mathcal{W}$, as fewer clusters are depleted. For long times, a reduction by α in the injection rate J_{on} results in a diminution of both $\mathcal{A}$ and $\mathcal{W}$. Interestingly, at short times, the change in J_{on} by a factor α yields an initial (transient) rise, regardless of the decrease in J_{off} by β. This can be explained by Taylor expanding $\mathcal{A}(\tau)$ and $\mathcal{W}(\tau)$ for small values. For instance, $\mathcal{A}(\tau) = \mathcal{A}(0) + \frac{1}{2}\tau a_S\phi_\infty(1 - \alpha) + \mathcal{O}[\tau^2]$, which shows that the linear term is positive if $\alpha < 1$ and independent of β. Although the expansion is more cumbersome in the case of $\mathcal{W}$, the same feature is preserved at first order (see SM).

Such an assay, as shown in fig. 2, could plausibility be performed experimentally by up-regulating or knocking down key elements of the synthesis or endocytic pathway. Since the relaxation times of the moments can be on the order of tens of minutes (cf. fig. 2), they can be measured

via single molecule super-resolution imaging techniques, such as stimulated emission depletion microscopy (STED), and photoactivated localization microscopy (PALM) [49]. This allows us to estimate J_{on} and J_{off} by comparison with the decay rates of (6) and (9). Another method that can be used to infer the recycling rates is to obtain experimentally the steady-state values of $\rho(\tau)$ and $\phi(\tau)$, namely $\rho_\infty = \mathcal{Q}_\infty - J_{\text{off}}$ and $\phi_\infty = J_{\text{on}}/J_{\text{off}}$, respectively. This can be particularly helpful if the experimental setup lacks the temporal resolution to measure the relaxation times.

The steady-state value of the density $\hat{\mathcal{P}}(\lambda, t)$ is given by $\hat{\mathcal{P}}_\infty(\lambda) = \mathcal{Q}_\infty - \mathcal{Q}_\lambda$, which can be exactly inverse Laplace transformed, and a closed-form solution is found to be

$$\mathcal{P}_\infty(a) = \frac{J_{\text{on}} e^{-a(1-\Omega)/a_S}}{a_S^2 \mathcal{Q}_\infty} \left[I_0\left(\frac{a\Omega}{a_S}\right) - I_1\left(\frac{a\Omega}{a_S}\right) \right], \quad (10)$$

where $\Omega = J_{\text{on}}/\mathcal{Q}_\infty^2$, and I_1 and I_0 are the modified Bessel functions of the first kind of order one and zero [51]. Figure 3(a) shows a few plots of eq. (10) for physiologically reasonable values of J_{on} and J_{off}. This further illustrates that small finite size domains can be found for a wide range of recycling rates (see inset plot of fig. 3). $\mathcal{P}_\infty(a)$ shows a power-law behaviour with an exponential cut-off [45], which is asserted by asymptotically expanding eq. (10),

$$\mathcal{P}_\infty(a) \simeq a^{-3/2} e^{-a/a_C} \sqrt{a_S J_{\text{on}}/(8\pi\Omega^2)}, \quad (11)$$

where $a_C = a_S(1 + 2J_{\text{on}}/J_{\text{off}}^2) \simeq 4\mathcal{A}_\infty^2/a_S$, and $\mathcal{A}_\infty$ is the steady-state value of the mean cluster size. As $a_C \gg \mathcal{A}_\infty$, the mean area lies within the power-law regime. Notice that the cut-off a_C corresponds to the size at which the intramembrane dynamics (governed by the diffusion constant D) becomes comparable to the recycling kinetics. Hence, the scaling of a_C on the rates J_{on} and J_{off} could also be deduced from dimensional analysis.

Biomembrane domains can exhibit various types of size distributions, reflecting distinct mechanisms of regulation and formation [49]. For instance, the power-law distribution in eq. (11) has been experimentally observed *in vivo* for the size of E-cadherin clusters, which has been measured by PALM microscopy [47–49]. The domains of E-cadherin are continuously recycled, and their size distribution shows an exponential cut-off for large clusters [47].

We now consider the size-dependent recycling scheme, where $f_{\text{off}} \neq 0$ in eq. (2). By Laplace transforming the governing equation and non-dimensionalising as done before, we derive a similar expression to eq. (4) with an additional term on the right-hand side of the equation that is given by $\mathcal{F}(\lambda, \tau) = F_{\text{off}}[\hat{\mathcal{P}}(\lambda_\star + \lambda, \tau) - \hat{\mathcal{P}}(\lambda, \tau)]$, with $F_{\text{off}} = f_{\text{off}} a_S/D$ and $\lambda_\star = a_S/a_L$. Thus, this leads to a nonlinear differential equation with a recurrence-like relation for the continuous variable λ. Such equations are difficult to solve exactly or even numerically. Nevertheless, further analytical progress can be made by assuming that the ratio $\lambda_\star \ll 1$ (typically $\lambda_\star \simeq 10^{-3}$), which yields that
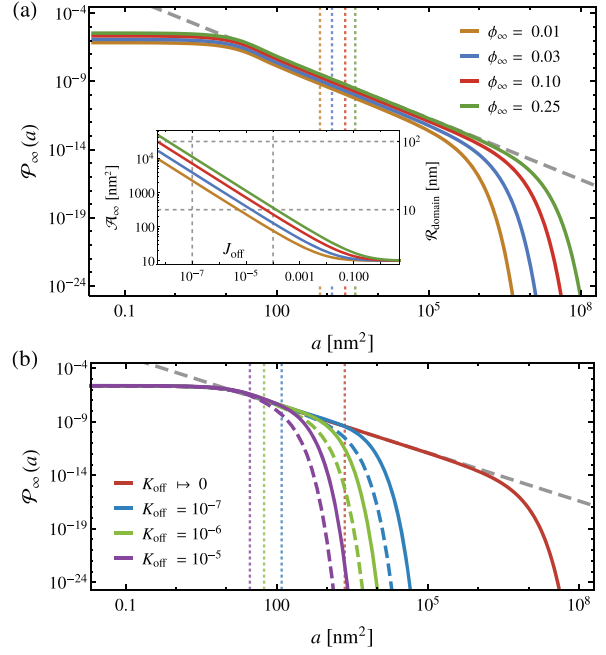

Fig. 3: (Color online) (a) Steady-state size distribution $\mathcal{P}_\infty(a)$ for the size-independent recycling at a fixed area coverage $\phi_\infty = J_{\text{on}}/J_{\text{off}}$. The recycling rate J_{off} is chosen such that the average area $\mathcal{A}_\infty$ from the distribution $\mathcal{P}_\infty(a)$ (as indicated by the vertical dotted lines) corresponds to the typical size of phase-separated domains observed in living cells, *i.e.*, $J_{\text{off}} = 10^{-6}$. The latter is found by plotting the mean area $\mathcal{A}_\infty$ as a function of J_{off} at a fixed area-fraction ϕ_∞, see the inset plot (same colours). The grey dashed lines are the upper and lower bounds to the physiological values of J_{off} and the area $\pi\mathcal{R}_{\text{domain}}^2$ of clusters. $\mathcal{P}_\infty(a)$ displays an exponential cut-off for large a, and a power-law behaviour, $\mathcal{P}_\infty(a) \sim a^{-3/2}$ for intermediate values ($a \gtrsim a_S$), as shown by the grey dashed line. (b) The steady-state distribution for a size-dependent recycling scheme, parametrized by the rate K_{off} (see text), with $J_{\text{on}} = 10^{-7}$ and $J_{\text{off}} = 10^{-6}$. This retrieves the size-independent case in the limit of $K_{\text{off}} = 0$, as shown by the red curve, which is equivalent to $\phi_\infty = 0.1$ of panel (a). This shows that a non-zero value of K_{off} decreases the size at which the domains are exponentially recycled, reducing the power-law regime (see the grey dashed line). The solid lines corresponds to $K_{\text{off}} > 0$, while the dashed curves are $K_{\text{off}} < 0$. When $|K_{\text{off}}| \gg J_{\text{off}}$, the distribution tends to an exponential function. The vertical dotted lines represent the mean domain sizes for $K_{\text{off}} > 0$ (same colour convention).

$\mathcal{F}(\lambda, \tau) = K_{\text{off}} \frac{\partial}{\partial\lambda} \hat{\mathcal{P}}(\lambda, \tau)$, with $K_{\text{off}} = \lambda_\star F_{\text{off}}$. Hence, the steady-state equation of $\hat{\mathcal{P}}(\lambda, \tau)$ is given by

$$K_{\text{off}} \frac{\partial\hat{\mathcal{P}}_\infty}{\partial\lambda} = (\rho_\infty + J_{\text{off}})\hat{\mathcal{P}}_\infty(\lambda) - \frac{1}{2}\hat{\mathcal{P}}_\infty^2(\lambda) - \frac{J_{\text{on}}}{1 + \lambda}, \quad (12)$$

which reduces to a special case of the associated Laguerre differential equation [51]. The solution of eq. (12) depends on the sign of K_{off}, and it can be written in terms of the Kummer function U of the second kind (if $K_{\text{off}} > 0$), and
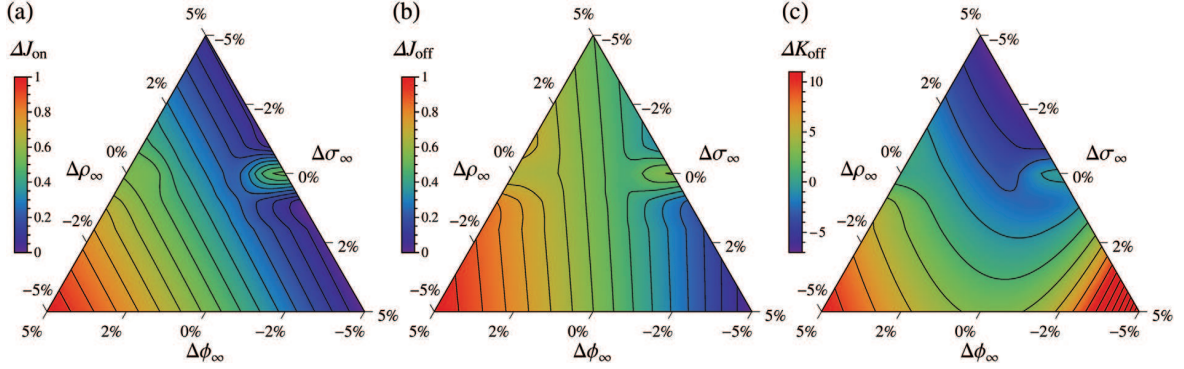
Fig. 4: (Color online) Ternary plots of the fractional changes (indicated by the prefix Δ) in (a) the injection rate around the value $J_{\mathrm{on}}^{(R)} = 10^{-5}$, (b) the size-independent removal rate about $J_{\mathrm{off}}^{(R)} = 10^{-4}$, and (c) the size-dependent outward rate around $K_{\mathrm{off}}^{(R)} = 10^{-8}$, which result from the fractional changes (or errors) in the moments of the steady-state domain size distribution; namely, the total number-per-area of clusters $\rho_{\infty}^{(R)} \approx 4 \times 10^{-3}$, their area-fraction $\phi_{\infty}^{(R)} \approx 0.1$, and the second moment $\sigma_{\infty}^{(R)} \approx 10^3$ of the distribution, which are computed in the linearised regime (see main text) for the values of the recycling rates mentioned above.

the generalized Laguerre function L (if $K_{\mathrm{off}} < 0$); namely,

$$
\hat{\mathcal{P}}_\infty(\lambda) = \begin{cases} \dfrac{J_{\mathrm{on}} U[1-\kappa; 1; (1+\lambda)\frac{\mathcal{I}}{\kappa}]}{K_{\mathrm{off}} U[-\kappa; 0; (1+\lambda)\frac{\mathcal{J}}{\kappa}]}, & K_{\mathrm{off}} > 0, \\[4mm] \dfrac{-J_{\mathrm{on}} L[\kappa-1; 0; (1+\lambda)\frac{\mathcal{J}}{\kappa}]}{\kappa K_{\mathrm{off}} L[\kappa; -1; (1+\lambda)\frac{\mathcal{J}}{\kappa}]}, & K_{\mathrm{off}} < 0, \end{cases}
\tag{13}
$$

where we also define that $\kappa = J_{\mathrm{on}}/[2K_{\mathrm{off}}(\rho_\infty + J_{\mathrm{off}})]$ and $\mathcal{J} = \frac{1}{2}J_{\mathrm{on}}/K_{\mathrm{off}}^2$ (see SM). Since these solutions depend on the undetermined constant ρ_∞, its value can be found by requiring the boundary condition $\rho_\infty = \hat{\mathcal{P}}_\infty(\lambda = 0)$, leading to a characteristic equation that needs to be solved first (see SM). Figure 3(b) shows the numerical inversion of the Laplace transform in eq. (13) using a multi-precision computing algorithm [52]. As $|K_{\mathrm{off}}|$ is increased, the exponential cut-off of the distribution is significantly decreased, diminishing the power-law regime over which the system is scale-free, as well as reducing the average domain size. Also, at fixed values of J_{on} and J_{off}, the critical area a_C and the mean area $\mathcal{A}_\infty$, when $K_{\mathrm{off}} < 0$, are both smaller than those found in the case of K_{off} being strictly positive.

For $K_{\mathrm{off}} > 0$, an asymptotic solution of eq. (13) can be found by expanding to first-order in $\lambda_\star$, resulting in

$$
\hat{\mathcal{P}}_\infty(\lambda) \simeq (\mathcal{Q}_\infty - \mathcal{Q}_\lambda)\left[1 + \frac{\Omega K_{\mathrm{off}} \mathcal{Q}_\infty}{J_{\mathrm{off}} \mathcal{Q}_\lambda^2}\right] - \frac{J_{\mathrm{on}} K_{\mathrm{off}}}{(1+\lambda)^2 \mathcal{Q}_\lambda^2}, \tag{14}
$$

which retrieves the previous result as $K_{\mathrm{off}} = 0$ (see SM). This can be exactly inverse Laplace transformed, which gives (see SM): $\mathcal{P}_\infty(a) = -K_{\mathrm{off}} a_S^{-2} e^{-a(1-\Omega)/a_S} \sinh(\frac{a\Omega}{a_S}) + \frac{J_{\mathrm{on}}}{\mathcal{Q}_\infty} a_S^{-2} e^{-a(1-\Omega)/a_S}[\Omega_+ I_0(\frac{a\Omega}{a_S}) - \Omega_- I_1(\frac{a\Omega}{a_S})] + \mathcal{O}[\lambda_\star^2]$, where $\Omega_\pm = 1 \pm \Omega K_{\mathrm{off}}/J_{\mathrm{off}}$. Also, from the derivatives of eq. (14) with respect to λ at zero, the moments of $\mathcal{P}$ can be computed (see SM). Thus, the linearised form in $\lambda_\star$ of the number-per-area of clusters is given by

$$
\rho_\infty \simeq \mathcal{Q}_\infty - J_{\mathrm{off}} - J_{\mathrm{on}} K_{\mathrm{off}}/(J_{\mathrm{off}} \mathcal{Q}_\infty) + O[\lambda_\star^2], \tag{15}
$$

and their area coverage is found to be

$$
\phi_\infty \simeq J_{\mathrm{on}}/J_{\mathrm{off}} - J_{\mathrm{on}} K_{\mathrm{off}}(J_{\mathrm{on}} + 2J_{\mathrm{off}}^2)/J_{\mathrm{off}}^4 + O[\lambda_\star^2]. \tag{16}
$$

Moreover, higher order moments may also be calculated, but their expressions become increasingly more cumbersome; for instance, the second moment is given by

$$
\begin{aligned}
\sigma_\infty \simeq & -J_{\mathrm{on}} K_{\mathrm{off}}(6J_{\mathrm{off}}^4 + 10J_{\mathrm{on}}J_{\mathrm{off}}^2 + 5J_{\mathrm{on}}^2)/J_{\mathrm{off}}^6 \\
& + J_{\mathrm{on}}(J_{\mathrm{on}} + 2J_{\mathrm{off}}^2)/J_{\mathrm{off}}^3 + O[\lambda_\star^2].
\end{aligned}
\tag{17}
$$

These moments are experimentally measurable, and this allows us to estimate the values of J_{on}, J_{off}, and K_{off} by simultaneously solving the eqs. (15), (16), and (17). To exemplify this inference problem, we study the response of the recycling rates to changes in the moments. Firstly, J_{on}, J_{off}, and K_{off} are selected such that they retrieve physiological values for the area-fraction and the mean area of domains. Namely, we choose $J_{\mathrm{on}}^{(R)} = 10^{-5}$, $J_{\mathrm{off}}^{(R)} = 10^{-4}$ and $K_{\mathrm{off}}^{(R)} = 10^{-8}$ as the reference values, which gives us that $\rho_\infty^{(R)} \approx 4 \times 10^{-3}$, $\phi_\infty^{(R)} \approx 0.1$ and $\sigma_\infty^{(R)} \approx 10^3$, resulting in an average area of membrane clusters $\mathcal{A}_\infty^{(R)} \approx 200$ nm^2. Here, we set $K_{\mathrm{off}}^{(R)}$ to be much smaller than the other rates, so that the linear regime in $\lambda_\star$ remains valid. By using $\mathcal{X}$ as a placeholder for the quantity of interest, we define the fractional change in $\mathcal{X}$ as follows $\Delta\mathcal{X} = (\mathcal{X}^{(R)} - \mathcal{X})/\mathcal{X}^{(R)}$. Secondly, we examine how a fractional change in the measured values of the moments, i.e., $\Delta\rho_\infty$, $\Delta\phi_\infty$ and $\Delta\sigma_\infty$, leads to a corresponding fractional variation in the rates around their reference values, inferred from eqs. (15)–(17). Lastly, to illustrate this, we project the points on a ternary diagram, as shown in fig. 4, so that the overall fractional variation is given by $\Delta\rho_\infty + \Delta\phi_\infty + \Delta\sigma_\infty = 5\%$. The plots show the sensitivity of the inferred rates to changes in the moments. In particular, we find that K_{off} exhibits larger changes about its reference value than the other rates.

Although the collision kernel $\mathcal{G}(a, a')$ has been regarded as a constant, this approximation breaks down, if the dilute limit is no longer satisfied, or if the size of the membrane domains $a \gg a_{\mathrm{SD}}$, as their diffusion coefficient now obeys the Stokes-Einstein relation ($D \sim a^{-1}$). By means of scaling arguments [44], and by also assuming that the coagulation kernel $\mathcal{G}$ is a homogeneous function of degree η, *i.e.*, $\mathcal{G}(a/\ell, a'/\ell) = \ell^{-\eta}\mathcal{G}(a, a')$, it can be shown that the steady-state distribution $\mathcal{P}_\infty(a) \sim a^{-\gamma}$, where the power-law exponent $\gamma = (3+\eta)/2$ [43]. For instance, if the diffusion of membrane clusters follows the Stokes-Einstein relation, we have $\mathcal{G}(a, a') \sim 1/a + 1/a'$, and thus we expect that $\mathcal{P}_\infty(a) \sim a^{-1}$. Note that this also retrieves our scaling result in eq. (11) when the exponent $\eta = 0$.

In summary, we developed an out-of-equilibrium model for the in-plane dynamics of membrane domains, where their stability and sizes are mediated by the exchange of membrane components with the exterior. The dynamics and the steady-states of the cluster size distribution are studied, subject to a size-dependent recycling. This model is sufficiently general, and can be applicable to a variety of other aggregation phenomena. Our analysis suggests a number of possible methods to experimentally test this model, and to generally assess the role of recycling in the formation and the control of membrane domains.

$$* * *$$

REFERENCES

[1] Engelman D. M., *Nature*, **438** (2005) 578.
[2] Kobayashi T., Gu F. and Gruenberg J., *Semin. Cell Dev. Biol.*, **9** (1998) 517.
[3] Hao M., *J. Biol. Chem.*, **275** (2000) 15279.
[4] Arumugam S. and Bassereau P., *Essays Biochem.*, **57** (2015) 109.
[5] Hancock J. F., *Nat. Rev. Mol. Cell Biol.*, **7** (2006) 456.
[6] Simons K. and Sampaio J. L., *Cold Spring Harbor Perspect. Biol.*, **3** (2011) a004697.
[7] Lavi Y., Edidin M. and Gheber L. A., *Biophys. J.*, **93** (2007) L35.
[8] Lenne P.-F. *et al.*, *Soft Matter*, **5** (2009) 2841.
[9] Greenfield D. *et al.*, *PLoS Biol.*, **7** (2009) e1000137.
[10] Destainville N., Schmidt T. H. and Lang T., *Curr. Top. Membr.*, **77** (2016) 27.
[11] Veatch S. L. and Keller S. L., *Biochim. Biophys. Acta*, **1746** (2005) 172.
[12] Bray A., *Adv. Phys.*, **43** (1994) 357.
[13] Yethiraj A. and Weisshaar J. C., *Biophys. J.*, **93** (2007) 3113.
[14] Liu J., Qi S., Groves J. T. and Chakraborty A. K., *J. Phys. Chem. B*, **109** (2005) 19960.
[15] Wallace E. J., Hooper N. M. and Olmsted P. D., *Biophys. J.*, **90** (2006) 4104.
[16] García-Sáez A. J., Chiantia S. and Schwille P., *J. Biol. Chem.*, **282** (2007) 33537.
[17] Lin Q. and London E., *J. Biol. Chem.*, **288** (2013) 1340.
[18] Baumgart T., Hess S. T. and Webb W. W., *Nature*, **425** (2003) 821.
[19] Ogunyankin M. O. and Longo M. L., *Soft Matter*, **9** (2013) 2037.
[20] Yamamoto T., Brewster R. and Safran S. A., *EPL*, **91** (2010) 28002.
[21] Brewster R. and Safran S. A., *Biophys. J.*, **98** (2010) L21.
[22] Hirose Y., Komura S. and Andelman D., *Phys. Rev. E*, **86** (2012) 021916.
[23] Palmieri B. *et al.*, *Adv. Colloid Interface Sci.*, **208** (2014) 58.
[24] Giang H., Shlomovitz R. and Schick M., *Essays Biochem.*, **57** (2015) 21.
[25] Leibler S. and Andelman D., *J. Phys. France*, **48** (1987) 2013.
[26] Rautu S. A., Rowlands G. and Turner M. S., *Phys. Rev. Lett.*, **114** (2015) 098101.
[27] Shlomovitz R. and Schick M., *Biophys. J.*, **105** (2013) 1406.
[28] Schick M., *Phys. Rev. E*, **85** (2012) 1.
[29] Honerkamp-Smith A. R., Veatch S. L. and Keller S. L., *Biochim. Biophys. Acta*, **1788** (2009) 53.
[30] Veatch S. L. *et al.*, *Proc. Natl. Acad. Sci. U.S.A.*, **104** (2007) 17650.
[31] Mayor S. and Rao M., *Traffic*, **5** (2004) 231.
[32] Gowrishankar K. *et al.*, *Cell*, **149** (2012) 1353.
[33] Tang Q. and Edidin M., *Biophys. J.*, **81** (2001) 196.
[34] Foret L., *Europhys. Lett.*, **71** (2005) 508.
[35] Gómez J., Sagués F. and Reigada R., *Phys. Rev. E*, **80** (2009) 011920.
[36] Foret L., *Eur. Phys. J. E*, **35** (2012) 12.
[37] Fan J., Sammalkorpi M. and Haataja M., *Phys. Rev. Lett.*, **104** (2010) 118101.
[38] Reigada R. and Mikhailov A. S., *Phys. Rev. E*, **93** (2016) 010401.
[39] Turner M. S., Sens P. and Socci N. D., *Phys. Rev. Lett.*, **95** (2005) 168301.
[40] Vagne Q., Turner M. S. and Sens P., *PLoS ONE*, **10** (2015) e0143470.
[41] Berger M., Manghi M. and Destainville N., *J. Phys. Chem. B*, **120** (2016) 10588.
[42] Davies S. C., King J. R. and Wattis J. A. D., *J. Eng. Math.*, **36** (1999) 57.
[43] Camacho J., *Phys. Rev. E*, **63** (2001) 046112.
[44] Leyvraz F., *Phys. Rep.*, **383** (2003) 95.
[45] Connaughton C. and Krapivsky P. L., *Phys. Rev. E*, **81** (2010) 035303(R).
[46] Lushnikov A. A., *Phys. At. Nucl.*, **74** (2011) 1096.
[47] Truong Quang B.-A. *et al.*, *Curr. Biol.*, **23** (2013) 2197.
[48] Wu Y., Kanchanawong P. and Zaidel-Bar R., *Dev. Cell*, **32** (2015) 139.
[49] Truong-Quang B.-A. and Lenne P.-F., *Front. Plant Sci.*, **5** (2014) 18.
[50] Saffman P. G. and Delbruck M., *Proc. Natl. Acad. Sci. U.S.A.*, **72** (1975) 3111.
[51] Abramowitz M. and Stegun I., *Handbook of Mathematical Functions* (Dover Pub., New York) 1965.
[52] Abate J. and Valk P. P., *Int. J. Numer. Methods Eng.*, **60** (2004) 979.